Inorg. Chem. **2007**, *46*, 8913–8923

Mononuclear Ni(II)-Thiolate Complexes with Pendant Thiol and Dinuclear Ni(III/II)-Thiolate Complexes with Ni···Ni Interaction Regulated by the Oxidation Levels of Nickels and the Coordinated Ligands

Chien-Ming Lee,[†] Tzung-Wen Chiou,[†] Hsin-Hung Chen,[†] Chao-Yi Chiang,[†] Ting-Shen Kuo,[‡] and Wen-Feng Liaw*,[†]

Department of Chemistry, National Tsing Hua University, Hsinchu 30043, Taiwan, Instrumentation Center, National Taiwan Normal University, Taipei, Taiwan

Received April 16, 2007

Compared to $[Ni^{II}(SePh)(P(o\text{-}C_6H_3\text{-}3\text{-}SiMe_3\text{-}2\text{-}S)_2(o\text{-}C_6H_3\text{-}3\text{-}SiMe_3\text{-}2\text{-}SH))]^-$ (**1a**) and $[Ni^{II}(Cl)(P(o\text{-}C_6H_3\text{-}3\text{-}SiMe_3\text{-}2\text{-}S)_2(o\text{-}C_6H_3\text{-}3\text{-}SiMe_3\text{-}2\text{-}SH))]^-$ (**3a**) with a combination of the intramolecular [Ni···H—S] and [Ni–S···H–S] interactions, complexes $[Ni^{II}(SePh)(P(o\text{-}C_6H_3\text{-}3\text{-}SiMe_3\text{-}2\text{-}S)_2(o\text{-}C_6H_3\text{-}3\text{-}SiMe_3\text{-}2\text{-}SH))]^-$ (**1b**) and $[Ni^{II}(Cl)(P(o\text{-}C_6H_3\text{-}3\text{-}SiMe_3\text{-}2\text{-}S)_2(o\text{-}C_6H_3\text{-}3\text{-}SiMe_3\text{-}2\text{-}SH))]^-$ (**3b**) with intramolecular [Ni···H–S] interaction exhibit lower ν_{S-H} stretching frequencies (2137 and 2235 cm^{-1} for **1b** and **3b** vs 2250 and 2287 cm^{-1} for **1a** and **3a**, respectively) and smaller torsion angles (27.2° for **3b** vs 58.9 and 59.1° for **1a** and **3a**, respectively). The pendant thiol interaction modes of **1a**, **3a**, and **3b** in the solid state are controlled by the solvent pairs of crystallization. Oxygen oxidation of dinuclear $[Ni^{II}(P(o\text{-}C_6H_3\text{-}3\text{-}SiMe_3\text{-}2\text{-}S)_2(o\text{-}C_6H_3\text{-}3\text{-}SiMe_3\text{-}2\text{-}SH))]_2$ (**4**) yielded thermally stable dinuclear $[Ni^{III}(P(o\text{-}C_6H_3\text{-}3\text{-}SiMe_3\text{-}2\text{-}S)_2(o\text{-}C_6H_3\text{-}3\text{-}SiMe_3\text{-}2\text{-}\mu\text{-}S))]_2$ (**5**). The two paramagnetic d^7 Ni^{III} cores ($S = {}^1/_2$) with antiferromagnetic coupling ($J = -3.13\ cm^{-1}$) rationalize the diamagnetic property of **5**. The fully delocalized mixed-valence [Ni(II)–Ni(III)] complexes $[Ni_2(P(o\text{-}C_6H_3\text{-}3\text{-}SiMe_3\text{-}2\text{-}S)_3)_2]^-$ (**6**) and $[Ni_2(P(o\text{-}C_6H_3\text{-}3\text{-}SiMe_3\text{-}2\text{-}S)_3)(P(o\text{-}C_6H_3\text{-}3\text{-}SiMe_3\text{-}2\text{-}S)_2(o\text{-}C_6H_3\text{-}3\text{-}SiMe_3\text{-}2\text{-}SCH_3))]$ (**7**) were isolated upon the reduction of **5** and the methylation of **6**, respectively. The electronic perturbation from the sulfur methylation of **6** triggers the stronger Ni···Ni interaction and the geometrical rearrangement from the diamond shape of the $[NiS_2Ni]$ core to the butterfly structure of $[Ni(\mu\text{-}S)_2Ni]$ to yield **7** with Ni···Ni distances of 2.6088(1) Å. The distinctly different Ni···Ni distances (2.6026(7) for **5** and 2.8289(15) Å for **6**) and the coordination number of the nickels indicate a balance of geometrical requirements for different oxidation levels of $[PS_3Ni–NiPS_3]$ cores of **5** and **6**.

Introduction

Hydrogenases catalyze a reversible two-electron oxidation of H_2 in aerobic and anaerobic microorganisms.[1] Two classes of hydrogenases, [Fe]-only hydrogenases ([Fe]-only H_2ases) and [NiFe] hydrogenases ([NiFe] H_2ases), have been studied widely.[1] The X-ray crystallographic studies of the active-site structure of [NiFe] hydrogenases isolated from *D. gigas*, *D. vulgaris*, *D. fructosovorans*, and *D. desulfuricans* ATCC27774 in combination with infrared spectroscopy have revealed an active site comprised of a heterobimetallic $(S_{cys})_2Ni(\mu\text{-}S_{cys})_2(\mu\text{-}X)Fe(CO)(CN)_2$ ($X = O^{2-}, HO_2^-, OH^-$) cluster (Figure 1).[2−5] The bridging ligand X was proposed

* To whom correspondence should be addressed. E-mail: wfliaw@mx.nthu.edu.tw.
[†] National Tsing Hua University.
[‡] National Taiwan Normal University.

(1) (a) Carepo, M.; Tierney, D. L.; Brondino, C. D.; Yang, T. C.; Pamplona, A.; Telser, J.; Moura, I.; Moura, J. J. G.; Hoffman, B. M. *J. Am. Chem. Soc.* **2002**, *124*, 281−286. (b) Albracht, S. P. J. *Biochim. Biophys. Acta* **1994**, *1188*, 167−204. (c) Adams, M. W. W.; Stiefel, E. I. *Curr. Opin. Chem. Biol.* **2000**, *4*, 214−220. (d) Fan, C.; Teixeira, M.; Moura, J.; Moura, I.; Huynh, B. H.; Le Gall, J.; Peck, H. D., Jr.; Hoffman, B. M. *J. Am. Chem. Soc.* **1991**, *113*, 20−24. (e) Whitehead, J. P.; Gurbiel, R. J.; Bagyinka, C.; Hoffman, B. M.; Maroney, M. J. *J. Am. Chem. Soc.* **1993**, *115*, 5629−5635.

(2) (a) Volbeda, A.; Charon, M. H.; Piras, C.; Hatchikian, E. C.; Frey, M.; Fontecilla-Camps, J. C. *Nature* **1995**, *373*, 580−587. (b) Garcin, E.; Vernede, X.; Hatchikian, E. C.; Volbeda, A.; Frey, M.; Fontecilla-Camps, J.-C. *Structure* **1999**, *7*, 557−566. (c) Happe, R. P.; Roseboom, W.; Pierik, A. J.; Albracht, S. P. J *Nature* **1997**, *385*, 126. (d) Volbeda, A.; Garcin, E.; Piras, C.; De Lacey, A. L.; Fernandez, V. M.; Hatchikian, E. C.; Frey, M.; Fontecilla-Camps, J. C. *J. Am. Chem. Soc.* **1996**, *118*, 12989−12996. (e) Volbeda, A.; Martin, L.; Cavazza, C.; Matho, M.; Faber, B. W.; Roseboom, W.; Albracht, S. P. J.; Garcin, E.; Rousset, M.; Fontecilla-Camps, J. C. *J. Biol. Inorg. Chem.* **2005**, *10*, 239−249.

10.1021/ic700719h CCC: $37.00
Published on Web 09/15/2007

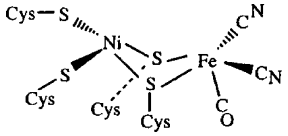

Figure 1. Schematic drawing of the active site of [NiFe] hydrogenases as deduced from crystallographic studies.[2]

to be an oxide, hydroxide, or hydro-peroxide in the oxidized state and was found to be absent in the reduced state. The coordination environment about nickel in the [NiFe] H_2ases is pseudo-tetrahedral in the reduced state and pseudo-square pyramidal in the oxidized state. The nickel site has been proposed to be redox active and changes between Ni(III) and Ni(II), whereas the iron site remains as Fe(II) in all of the spectrally defined redox states of the enzyme.[2−5] The active center of [NiFe] H_2ase exhibits various redox states in the hydrogen catalytic cycle. The EXAFS/EPR studies indicate that the formal oxidation state of the nickel center is paramagnetic Ni(III) in Ni−A, Ni−B, and Ni−C states.[2−5] The Ni−A and Ni−B states can be converted into the reduced forms Ni−SU and Ni−SI via one-electron reduction, respectively. The Ni−SI state transforms into the EPR-silent, active state Ni−SIa, which can then be reduced to the EPR-detectable Ni−C state. Actually, the active form Ni−C (the paramagnetic Ni−C intermediate) of [NiFe] H_{2ase} was proposed to exist as the $[(S_{cys}-H)Ni^{III}-H-Fe]$ intermediates after an active state Ni−SIa (silent-active $[(S_{cys}-H)Ni^{II}(S_{cys})_3]$) is passed. Ni−R/Ni−SIa states were proposed to exist as $[(S_{cys}-H)(S_{cys})Ni^{II}(\mu\text{-}S_{cys})_2Fe(CO)(CN)_2]$ with a Cys−SH interacting directly with the nickel center (a $[Ni\cdots H-S_{cys}]$ interaction).[2−5] In particular, recent X-ray absorption spectroscopy shows that the nickel site of the regulatory hydrogenase (RH) in the presence of hydrogen (RH^{+H2}), proposed as the Ni−C state, isolated from *Ralstonia eutropha* is a six-coordinated $[Ni^{III}-S_2(O/N)_3(H)]$.[6]

In model compounds, the kinetics studies of the protonation of complex $[BPh_4]$ [Ni(SEt)(triphos)] (triphos = $(Ph_2PCH_2CH_2)_2PPh$) revealed that the sulfur atom is the initial site for the protonation of $[BPh_4][Ni(SEt)(triphos)]$, and the interaction of the proton with both the nickel and sulfur sites

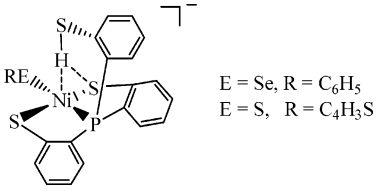

Figure 2. Schematic drawing of $[PPN][Ni^{II}(ER)(P(o\text{-}C_6H_3S)_2(o\text{-}C_6H_3SH))]$.[11]

(an η^2-EtS−H complex) was proposed.[7] $Ni^{II}(Bm^{Me})_2$ (Bm^{Me}=bis-(2-mercapto-1-methyl-imidazolyl) borate) with a $[NiS_4H_2]$ core and the presence of the Ni···H−B interaction may provide a structural model of the nickel site of [NiFe]H_2-ase.[8] The EPR and single-crystal X-ray structure provided evidence for the formation of dinuclear [Ni(II)Ni(III)]-thiolate complexes generated by one-electron oxidation of a dinuclear Ni(II)-macrocyclic complex $[Bu_4N]_2[Ni_2(E)]$ (E = macrocyclic ligand)[9a] and $[Bu_4N]_2[Ni_2\{P(o\text{-}C_6H_4S)_3\}_2]$,[9b] respectively. Recently, a number of $[Ni^{II}-Fe]$ model compounds were reported.[10] However, the investigation of the relationship between the core geometry of the bimetallic [Ni−Fe]/[Ni−Ni] center and the oxidation levels of nickel is limited.

In the previous study, we reported the syntheses and characterizations of the mononuclear $[PPN][Ni^{II}(L)(P(o\text{-}C_6H_4S)_2(o\text{-}C_6H_4SH))]$ and $[PPN][Ni^{III}(L)(P(o\text{-}C_6H_4S)_3)]$ (L = SePh, SEt, Cl) (Figure 2).[11] In this article, the thermally stable complexes $[PPN][Ni^{II}(L)(P(o\text{-}C_6H_3\text{-}3\text{-}SiMe_3\text{-}2\text{-}S)_2(o\text{-}C_6H_3\text{-}3\text{-}SiMe_3\text{-}2\text{-}SH))]$ (L = SePh (**1a**, **1b**), Cl (**3a**, **3b**)) were synthesized to elucidate the modes of the intramolecular [Ni−S···H−S]/[Ni···H−S] interactions regulated by the solvent pairs of crystallization. A series of dinuclear nickel complexes $[Ni^{II}(P(o\text{-}C_6H_3\text{-}3\text{-}SiMe_3\text{-}2\text{-}S)_2(o\text{-}C_6H_3\text{-}3\text{-}SiMe_3\text{-}2\text{-}SH))]_2$ (**4**), $[Ni^{III}(P(C_6H_3\text{-}3\text{-}SiMe_3-2\text{-}S)_2(C_6H_3\text{-}3\text{-}SiMe_3\text{-}2\text{-}\mu\text{-}S))]_2$ (**5**), and the mixed-valence [Ni(II)−Ni(III)] complexes [Na-18-crown-6-ether]$[Ni_2(P(o\text{-}C_6H_3\text{-}3\text{-}SiMe_3\text{-}2\text{-}S)_3)_2]$ (**6**) and $[Ni_2(P(o\text{-}C_6H_3\text{-}3\text{-}SiMe_3\text{-}2\text{-}S)_3)(P(o\text{-}C_6H_3\text{-}3\text{-}SiMe_3\text{-}2\text{-}S)_2(o\text{-}C_6H_3\text{-}3\text{-}SiMe_3\text{-}2\text{-}SCH_3))]$ (**7**), and the dianionic dinuclear $[K\text{-}18\text{-}crown\text{-}6\text{-}ether]_2[Ni^{II}_2(P(o\text{-}C_6H_3\text{-}3\text{-}SiMe_3\text{-}2\text{-}S)_3)_2]$ (**8**) were isolated and characterized to study the correlation among the presence/absence of Ni···Ni interac-

(3) (a) Higuchi, Y.; Yagi, T.; Yasuoka, N. *Structure* **1997**, *5*, 1671−1680. (b) Higuchi, Y.; Ogata, H.; Miki, K.; Yasuoka, N.; Yagi, T. *Structure* **1999**, *7*, 549−556. (c) Ogata, H.; Mizoguchi, Y.; Mizuno, N.; Miki, K.; Adachi, S.-I.; Yasuoka, N.; Yagi, T.; Yamauchi, O.; Hirota, S.; Higuchi, Y. *J. Am. Chem. Soc.* **2002**, *124*, 11628−11635. (d) Foerster, S.; Stein, M.; Brecht, M.; Ogata, H.; Higuchi, Y.; Lubitz, W. *J. Am. Chem. Soc.* **2003**, *125*, 83−93. (e) Ogata, H.; Hirota, S.; Nakahara, A.; Komori, H.; Shibata, N.; Kato, T.; Kano, K.; Higuchi, Y. *Structure* **2005**, *13*, 1635−1642.

(4) (a) Rousset, M.; Montet, Y.; Guigliarelli, B.; Forget, A.; Asso, M.; Bertrand, P.; Fontecilla-Camps, J. C.; Hatchikian, E. C. *Proc. Natl. Acad. Sci. U.S.A.* **1998**, *95*, 11625−11630. (b) Tye, J. W.; Hall, M. B.; Darensbourg, M Y. *Proc. Natl. Acad. Sci. U.S.A.* **2005**, *102*, 16911−16912.

(5) (a) Maroney, M. J.; Davidson, G.; Allan, C. B.; Figlar, J. S*truct. Bond.* **1998**, *92*, 1−65. (b) Stein, M. M.; Lubitz, W. *Curr. Opin. Chem. Biol.* **2002**, *6*, 243−249. (c) Lamle, S. E.; Albracht, S. P.; Armstrong, F. A. *J. Am. Chem. Soc.* **2005**, *127*, 6595−6604. (d) Matias, P. M.; Soares, C. M.; Saraiva, L. M.; Coelho, R.; Morais, J.; Le Gall, J.; Carrondo, M. A. *J. Biol. Inorg. Chem.* **2001**, *6*, 63−81.

(6) (a) Haumann, M.; Porthum, A.; Buhrke, T.; Liebisch, P.; Meyer-Klaucke, W.; Friedrich, B.; Dau, H. *Biochemistry* **2003**, *42*, 11004−11015. (b) Brecht, M.; Gastel, M. V.; Buhrke, T.; Friedrich, B.; Lubitz, W. *J. Am. Chem. Soc.* **2003**, *125*, 13075−13083.

(7) Clegg, W.; Henderson, R. A. *Inorg. Chem.* **2002**, *41*, 1128−1135.

(8) Alvarez, H. M.; Krawiec, M.; Donovan-Merkert, B. T.; Fouzi, M.; Rabinovich, D. *Inorg. Chem.* **2001**, *40*, 5736−5737.

(9) (a) Branscombe, N. D. J.; Atkin, A. J.; Marin-Becerra, A.; McInnes, E. J. L.; Mábbs, F. E.; McMaster, J; Schröder, M. *Chem. Commun.* **2003**, 1098−1099. (b) Franolic, J. D.; Wang, W. Y.; Millar, M. *J. Am. Chem. Soc.* **1992**, *114*, 6587−6588.

(10) (a) Bouwan, E.; Reedijk, J. *Coord. Chem. Rev.* **2005**, *249*, 1555−1581 and reference therein. (b) Brecht, M.; Gastel, M.; Buhrke, T.; Friedrich, B.; Lubitz, W. *J. Am. Chem. Soc.* **2003**, *125*, 13075−13083. (c) Branscombe, N. D. J.; Atkins, A. J.; Marin-Becerra, A.; McInnes, E. J. L.; Mabbs, F. E.; McMastera, J.; Schröder, M. *Chem. Commun.* **2003**, 1098−1099. (d) Ogo, S.; Kabe, R.; Uehara, K.; Kure, B.; Nishimura, T.; Menon, S. C.; Harada, R.; Fukuzumi, S.; Higuchi, Y.; Ohhara, T.; Tamada, T.; Kuroki, R. *Science* **2007**, *316*, 585−587. (e) Sellmann, D.; Lauderbach, F.; Heinemann, F. W. *Eur. J. Inorg. Chem.* **2005**, 371−377. (f) Zhu, W.; Marr, A. C.; Wang, Q.; Neese, F.; Spencer, D. J. E.; Blake, A. J.; Cooke, P. A.; Wilson, C.; Schröder, M. *Proc. Natl. Acad. Sci. U.S.A.* **2005**, *102*, 12820−12825.

(11) (a) Lee, C.-M.; Chen, C.-H.; Ke, S.-C.; Lee, G.-H.; Liaw, W.-F. *J. Am. Chem. Soc.* **2004**, *126*, 8406−8412. (b) Chen, C.-H.; Lee, G.-H.; Liaw, W.-F. *Inorg. Chem.*, **2006**, *45*, 2307−2316. (c) Lee, C.-M.; Chuang, Y.-L.; Chiang, C.-Y.; Lee, G.-H.; Liaw, W.-F. *Inorg. Chem.* **2006**, *45*, 10895−10904.

Scheme 1

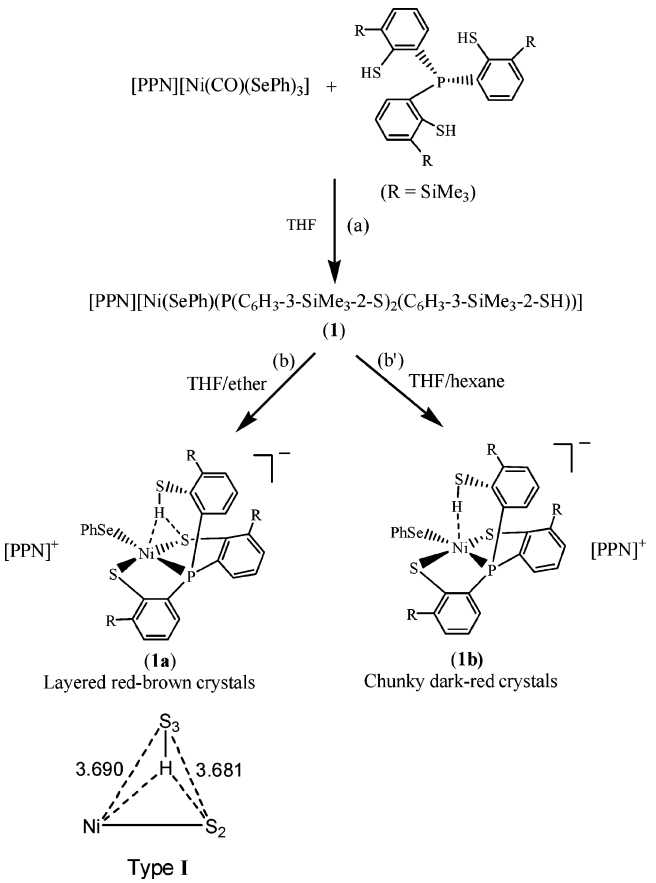

tion, the geometry of [$PS_3Ni-NiS_3P$] core, and the electronic states (electronic density) of [$PS_3Ni-NiS_3P$] cores of complexes.

Results and Discussion

The Pendant Thiol Interaction Modes of Complex [PPN][Ni(SePh)(P(*o*-C_6H_3-3-$SiMe_3$-2-S)$_2$(*o*-C_6H_3-3-$SiMe_3$-2-SH))] (1a/1b). As reported in the previous study, the reaction of [PPN][Ni(CO)(SePh)$_3$] and P(*o*-C_6H_3-3-$SiMe_3$-2-SH)$_3$ led to the formation of [PPN][Ni(SePh)(P(*o*-C_6H_3-3-$SiMe_3$-2-S)$_2$(*o*-C_6H_3-3-$SiMe_3$-2-SH))] (**1**), isolated as a dark red-brown solid (85% yield) (Scheme 1a).[11c] In contrast to the analogue [PPN][Ni(SePh)(P(*o*-C_6H_4-2-S)$_2$(*o*-C_6H_4-2-SH))] (**2**),[11] **1** coordinated with the trimethylsilyl-substituted [P(*o*-C_6H_3-3-$SiMe_3$-2-S)$_3$]$^{3-}$ ligand was soluble in THF. Two forms of crystalline products, **1a** (plate-shaped, red-brown crystals) and **1b** (block-shaped, dark-red crystals), were obtained when **1** was recrystallized from THF-diethyl ether and THF-hexane, respectively, at room temperature, as shown in parts b and b′ of Scheme 1′. The IR spectrum of **1a** in the solid-state reveals one stretching band (2250 cm^{-1} (KBr)) in the ν_{S-H} region, compared to **1b**, which displays a lower-energy ν_{S-H} stretching band (2137 cm^{-1} (KBr)). In comparison with free ligand P(*o*-C_6H_3-3-$SiMe_3$-2-SH)$_3$ (ν_{S-H}= 2466 cm^{-1} (KBr))(Table 1), the shifts of ν_{S-H} stretching frequencies in **1a** and **1b** imply the specific intramolecular [Ni···H−S]/[Ni−S···H−S] interactions.[11c]

In THF-d_8 solution, however, **1a** and **1b** exhibit identical ^{1}H NMR spectra at 25 °C, with thiol proton resonance at δ 8.59 (br) ppm under an N_2 atmosphere (Table 1). This study suggests that **1a** and **1b** are in dynamic equilibrium in solution and supports the existence of intramolecular [Ni···H−S]/[Ni−S···H−S] interactions, resulting in the ^{1}H NMR chemical shift of the SH group, from δ 4.58 (br) ($CDCl_3$) in free ligand P(*o*-C_6H_3-3-$SiMe_3$-2-SH)$_3$ to δ 8.59 (br) (SH) (C_4D_8O) in **1** (Table 1).

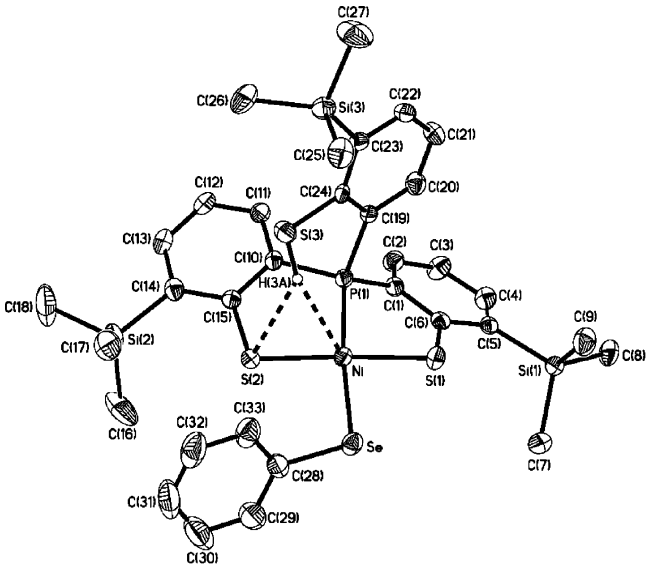

Figure 3. ORTEP drawing and labeling scheme of **1a** with thermal ellipsoids drawn at 30% probability level. Selected bond distances (Å) and angles (°): Ni−Se 2.3213(6), Ni(1)−S(1) 2.2096(11), Ni(1)−S(2) 2.1755(11), Ni(1)···S(3) 3.690(1), S(2)···S(3) 3.681(1), Ni−P(1) 2.0972(11), S(1)−Ni(1)−S(2) 162.26(4), S(1)−Ni(1)−Se 89.10(3), S(1)−Ni(1)−P(1) 84.99(4), S(2)−Ni(1)−Se 96.43(3), S(2)−Ni(1)−P(1) 89.55(4), Se−Ni−P(1) 174.00(4).

Table 1. IR ν_{S-H} Stretching Frequencies and ^{1}H NMR Chemical Shifts (δ_{S-H}) for [P(*o*-C_6H_3-3-$SiMe_3$-2-SH)$_3$] (P(S′H)$_3$), **1a**, **1b**, **3a**, **3b**, and **4**

complexes/ spectroscopic data	ν_{S-H}, cm^{-1} (KBr)	δ_{S-H}, ppm ($CDCl_3$)
P(S′H)$_3$	2466	4.58(br)
1a	2250	8.59(d)
1b	2137	8.59(d)
3a	2287	8.54(d)
3b	2235	8.54(d)
4	2385	6.24(d)

1a and **1b** were found to be the same monoclinic $P2_1/c$ space group but in the different unit cell dimensions. As shown in Figure 3, the acute ∠C(24)−S(3)−H(3S) bond angle of 96(2)° in **1a** is believed to result from an intramolecular [Ni···H−S]/[Ni−S···H−S] interaction (Scheme 1, Type **I**). The pendant thiol interaction modes in the solid state are ascribed to solvent effects during recrystallization. Diffusion of the less-polar solvent hexane into the THF solution of **1** yielded **1b**. Diffusion of *n*-hexane into a THF−H_2O solution (10:0.2 mL) of **1**, bearing comparison with diffusion of diethyl ether into THF solution of **1**, gave the layered, red-brown crystals identified as **1a**. The pendant thiol proton of **1a** is partially polarized and approaches the second sulfur atom. It can be interpreted in terms of the thiol proton interacting with both sulfur and nickel atoms, where the proton is bound to sulfur (S(3)) and attracted by Ni(II) and sulfur (S(2)) atoms, that is, a combination of [Ni···H−S] and [Ni−S···H−S] interactions (Scheme 1, Type **I**). How-

Scheme 2

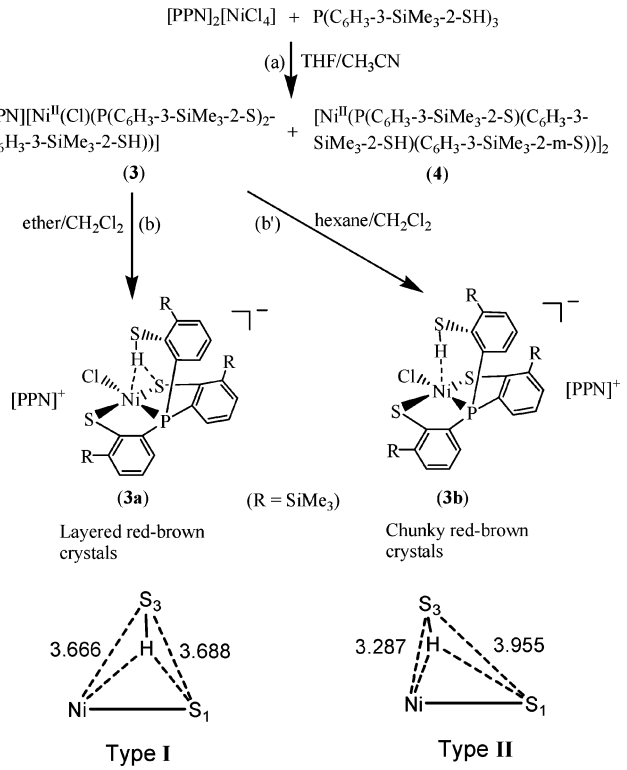

ever, the X-ray structure of **1b** is not of suitable quality for this publication.

The Pendant Thiol Interaction Modes of Mononuclear [PPN][Ni^{II}(Cl) (P(*o*-C$_6$H$_3$-3-SiMe$_3$-2-S)$_2$(*o*-C$_6$H$_3$-3-SiMe$_3$-2-SH))] (3a and 3b) in the Solid State. When P(*o*-C$_6$H$_3$-3-SiMe$_3$-2-SH)$_3$ (0.1 mmol) and [PPN]$_2$[NiCl$_4$] (0.1 mmol) were dissolved in THF−CH$_3$CN (5:0.5 mL volume ratio) at room temperature, a reaction ensued over the course of 30 min to give the mononuclear [PPN][Ni(Cl)(P(*o*-C$_6$H$_3$-3-SiMe$_3$-2-S)$_2$(*o*-C$_6$H$_3$-3-SiMe$_3$-2-SH))] (**3**) (yield 65%) after separation of the neutral [Ni(P(*o*-C$_6$H$_3$-3-SiMe$_3$-2-S)$_2$(*o*-C$_6$H$_3$-3-SiMe$_3$-2-SH))]$_2$ (**4**) (yield 25%) by hexane (Scheme 2). **3** is soluble in CH$_2$Cl$_2$ and is extremely O$_2$-sensitive in solution. Two types of crystalline products, layered red-brown (**3a**) and chunky red-brown (**3b**) crystals, were isolated upon diffusion of diethyl ether into the CH$_2$Cl$_2$ solution of **3** and diffusion of hexane into the CH$_2$Cl$_2$ solution of **3**, respectively, at room temperature (parts b and b′ of Scheme 2′).

Molecular structures of **3a** and **3b** are shown in parts a and b of Figure 4, respectively, and selected bond lengths and bond angles are collected in figure captions. The geometry of the nickel center in **3a** containing 0.5 THF solvent in crystal lattice is distorted square planar (ClPS$_2$) with the pendant thiol proton attracted by Ni(II) and sulfur, that is, a combination of intramolecular [Ni···H−S] and [Ni−S···H−S] interactions (Type **I**, as shown in Scheme 2 and the graphic). The ∠Ni−P(1)−C(14)−C(13) torsion angle of 59.1° in **3a** is significantly larger than that of ∠Ni(1)−P(1)−C(19)−C(20) (27.2°) in **3b**. In particular, the S(3)···Ni distance of 3.666(1) Å in **3a** is longer than that of 3.287(1) Å in **3b** (types **I** and **II**, as shown in Scheme 2 and the graphic).

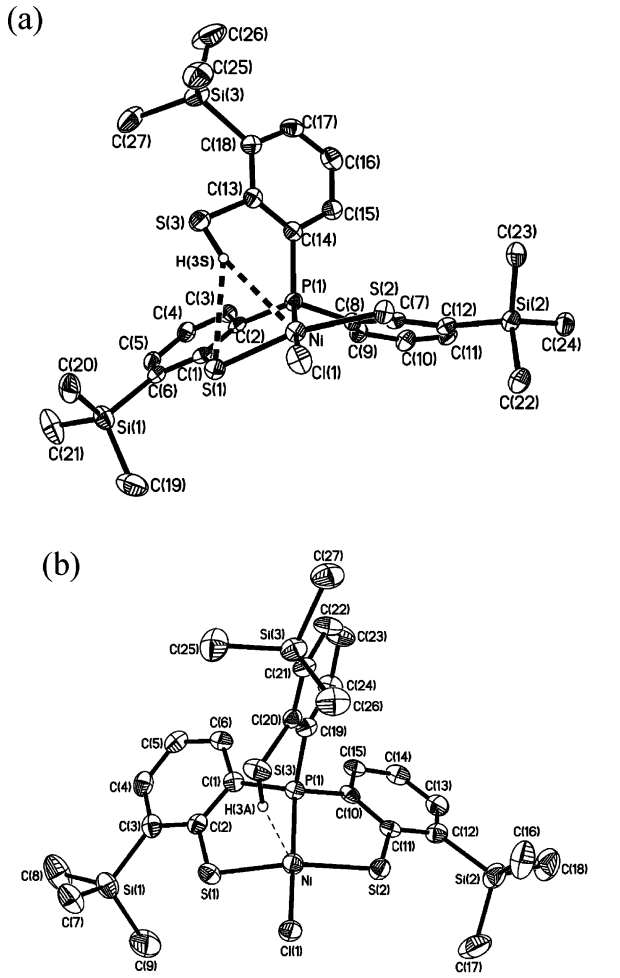

Figure 4. ORTEP drawing and labeling scheme of (a) **3a**, and (b) **3b** with thermal ellipsoids drawn at 30% probability level. Selected bond distances (Å) and angles (°): **3a**: Ni−Cl(1) 2.217(14), Ni(1)−S(1) 2.190(13), Ni(1)−S(2) 2.204(13), Ni(1)···S(3) 3.66(1), S(1)···S(3) 3.68(1), Ni−P(1) 2.087(14); S(1)−Ni−S(2) 163.3(6), S(1)−Ni−Cl(1) 93.6(5), S(1)−Ni−P(1) 89.3(5), S(2)−Ni−Cl(1) 93.7(5), S(2)−Ni−P(1) 84.6(5), Cl(1)−Ni−P(1) 175.0(6). **3b**: Ni−Cl(1) 2.2243(9), Ni(1)−S(1) 2.1570(10), Ni(1)−S(2) 2.1649(10), Ni(1)···S(3) 3.287(1), S(1)···S(3) 3.955(1), Ni−P(1) 2.0962(10); S(1)−Ni−S(2) 154.94(4), S(1)−Ni−Cl(1) 93.96(4), S(1)−Ni−P(1) 89.97(4), S(2)−Ni−Cl(1) 94.45(4), S(2)−Ni−P(1) 88.07(4), Cl(1)−Ni−P(1) 164.77(4).

As shown in Table 1, the IR ν_{S-H} stretching frequencies of **1a**, **1b**, **3a**, and **3b** are significantly disturbed by the monodentate coordinated ligands, [SePh]$^-$/[Cl]$^-$, and the pendant thiol proton interaction modes. The ν_{S-H} stretching frequencies (2250 and 2137 cm^{-1}, respectively) of **1a** and **1b** with the [SePh]$^-$ coordinated ligand are lower than those of **3a** (2287 cm^{-1}) and **3b** (2235 cm^{-1}), ligated by [Cl]$^-$. Of importance, the ν_{S-H} difference of 113 cm^{-1} between **1a** and **1b** is significantly larger than that of 52 cm^{-1} between **3a** and **3b**. These results support that an increase in the nickel electronic density modulated by the monodentate ligand attracts the proton of the pendant thiol effectively and causes the weaker S−H bond. This result is consistent with the higher pK_a of HSePh (pK_a = 7.1) than HCl (pK_a = 1.8) in dimethyl sulfoxide.[12]

(12) Bordwell, F. G. *Acc. Chem. Res.* **1988**, *21*, 456−463.

Scheme 3

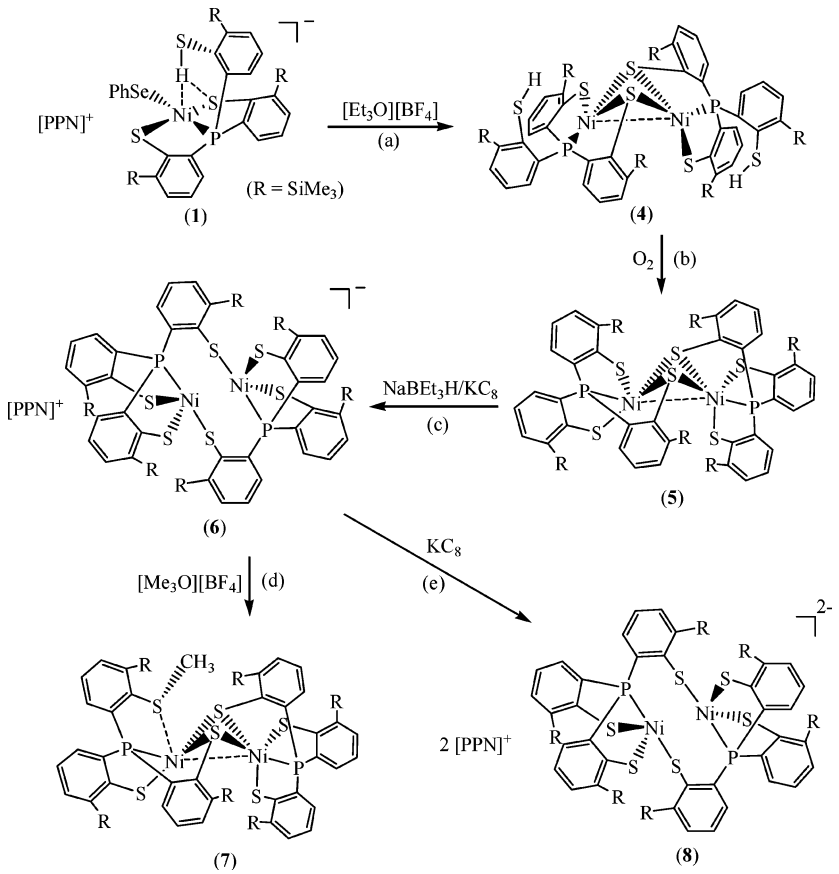

Both **3a** and **3b** exhibit identical ^{1}H NMR spectra, with the thiol protons resonances at δ 8.54 (br) (C_4D_8O) under a N_2 atmosphere (Table 1). It is noticed that the upfield chemical shift of the pendant thiol proton from δ 8.59 (**1**) to 8.54 (**3**) is consistent with ν_{S-H} stretching frequencies shifted from 2250/2137 (**1a**/**1b)** to 2287/2235 cm^{-1} (**3a**/**3b)** (KBr).

Neutral Dinuclear [Ni^{II}(P(*o*-C$_6$H$_3$-3-SiMe$_3$-2-S)$_2$(*o*-C$_6$H$_3$-3-SiMe$_3$-2-SH))]$_2$ (4) and [Ni^{III}(P(*o*-C$_6$H$_3$-3-SiMe$_3$-2-S)$_2$-(*o*-C$_6$H$_3$-3-SiMe$_3$-2-μ-S))]$_2$ (5). Compared to the reaction of P(*o*-C$_6$H$_3$-3-SiMe$_3$-2-SH)$_3$ and [NiCl$_4$]$^{2-}$, reaction of P(*o*-C$_6$H$_3$-3-SiMe$_3$-2-SH)$_3$ (0.1 mmol) and NiCl$_2$·6H$_2$O (0.1 mmol) yielded the neutral dinuclear Ni(II) complex [Ni(P(*o*-C$_6$H$_3$-3-SiMe$_3$-2-S)$_2$(*o*-C$_6$H$_3$-3-SiMe$_3$-2-SH))]$_2$ (**4**) in THF at ambient temperature. Alternatively, treatment of **1** (0.133 g, 0.1 mmol) with [Et$_3$O][BF$_4$] (0.1 mmol) in THF at 5 °C also led to the formation of **4** (yield 70%), accompanied by insoluble [PPN][BF$_4$] solid (part a of Scheme 3). Presumably, alkylation by electrophile ([Et$_3$O][BF$_4$]) occurs at the more accessible [SePh]$^-$ site, followed by coordinative association of two neutral [Ni^{II}(P(*o*-C$_6$H$_3$-3-SiMe$_3$-2-S)$_2$(*o*-C$_6$H$_3$-3-SiMe$_3$-2-SH))] units to produce **4**. **4** exhibits extreme air sensitivity in solution (THF, diethyl ether). Compared to complexes **1a**/**1b** (IR ν_{S-H} 2250 and 2137 cm^{-1} (KBr)) and **3a**/**3b** (IR ν_{S-H} 2287 and 2235 cm^{-1} (KBr)), the higher ν_{S-H} stretching frequency (2385 cm^{-1} (KBr)) of **4** implies the absence of intramolecular [Ni−S···H−S] interactions (Table 1). The ^{1}H NMR spectrum of **4** in $CDCl_3$ shows the thiol proton resonances at δ 6.24(d), a ∼1.66 ppm downfield shift compared to the free ligand. Three singlets (at δ 0.51, 0.33, and −0.11), derived from the protons of three trimethylsilyl groups, indicate that trimethylsilyl groups of **4** are not equivalent. The ^{2}H NMR spectrum (δ 6.37 (br) (C_4H_8O) (S−D)) and IR ν_{S-D} spectrum (1748 (br) cm^{-1} (υ_{S-D}, KBr)) demonstrated that the pendant thiol proton of **4** is D_2O exchangeable.

The single-crystal X-ray structure of **4** is shown in Figure 5, and selected bond distances and angles are collected in the figure caption. The elongation of Ni(1)···S(3)H(3A) and Ni(2)···S(6)H(6A) distances (3.947(1) and 3.868(1) Å, respectively) in **4**, compared to the Ni···S(3)H distance of 3.690(1) and 3.305(1) Å in **1a** and **1b**, respectively, also implicates the absence of the intramolecular [Ni−S···H−S] interactions. Formation of **4** via the coordinative association of two [Ni^{II}P(*o*-C$_6$H$_3$-3-SiMe$_3$-2-S)$_2$(*o*-C$_6$H$_3$-3-SiMe$_3$-2-SH)] units can lend support to the previous proposal that the distinct electron-donating ability of the coordinated ligands may serve to regulate the intramolecular [Ni−S···H−S]/[Ni···H−S] interactions.[11] The geometry about both of the central Ni(II) can be regarded as slightly distorted square planar. The dihedral angle between the two planes (Ni(1)S-(1)S(2) and Ni(2)S(1)S(2)) is 78.1° (Supporting Information Table S1), and the Ni(1)···Ni(2) distance of 2.5808(8) Å is short enough to suggest a certain degree of interaction between the two Ni(II) centers of **4**. Compared to the known nickel dimer (Supporting Information Table S1),[13] the short Ni(1)···Ni(2) distance found in **4** may be attributed to the electron deficiency of Ni(II) centers derived from the less electron-donating [P(*o*-C$_6$H$_3$-3-SiMe$_3$-2-S)$_2$(*o*-C$_6$H$_3$-3-SiMe$_3$-

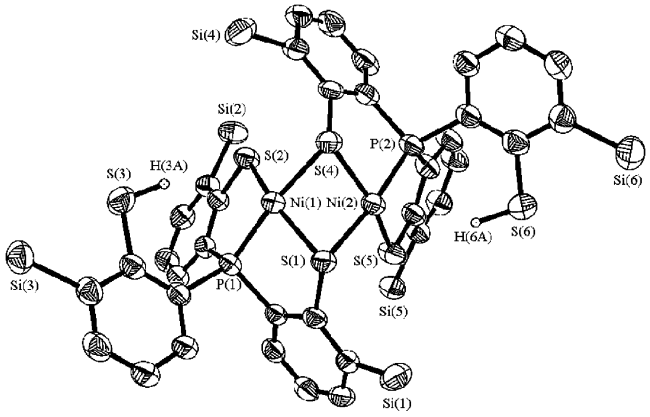

Figure 5. ORTEP drawing and labeling scheme of **4** with thermal ellipsoids drawn at 30% probability level (Me groups of $SiMe_3$ were omitted for clarity). Selected bond distances (Å) and angles (°): Ni(1)−S(1) 2.2078-(13), Ni(1)−S(4) 2.2696(12), Ni(1)−S(2) 2.1557(13), Ni(1)−S(3) 3.947-(1), Ni(1)−P(1) 2.1062(13), Ni(1)···Ni(2) 2.5808(8); S(1)−Ni(1)−S(2) 158.14(6), S(1)−Ni(1)−S(4) 84.01(4), S(2)−Ni(1)−S(4) 98.74(5), S(1)−Ni(1)−P(1) 87.45(5), S(2)−Ni(1)−P(1) 89.42(5), S(4)−Ni(1)−P(1) 171.43-(5), Ni(2)−S(4)−Ni(1) 70.33(4), Ni(1)−S(1)−Ni(2) 70.59(4).

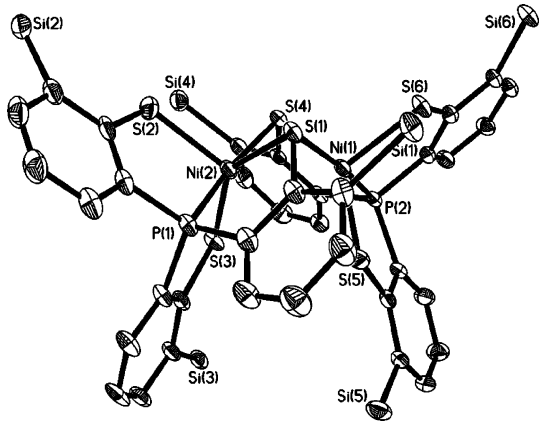

Figure 6. ORTEP drawing and labeling scheme of **5** with thermal ellipsoids drawn at 30% probability level (Me groups of $SiMe_3$ were omitted). Selected bond distances (Å) and angles (°): Ni(1)−S(1) 2.2529-(11), Ni(1)−S(4) 2.2837(11), Ni(1)−S(5) 2.2143(11), Ni(1)−S(6) 2.2722-(11), Ni(1)−P(2) 2.1271(11), Ni(1)···Ni(2) 2.6026(7); S(1)−Ni(1)−S(4) 87.3(4), S(1)−Ni(1)−S(5) 95.40(4), S(1)−Ni(1)−S(6) 98.32(4), S(1)−Ni-(1)−P(2) 172.11(4), S(4)−Ni(1)−P(2) 86.27(4), S(4)−Ni(1)−S(6) 102.73-(4), S(1)−Ni(1)−S(6) 98.32(4), S(5)−Ni(1)−S(6) 115.07(5), S(5)−Ni(1)−P(2) 86.78(4), S(6)−Ni(1)−P(2) 87.57(4), Ni(1)−S(1)−Ni(2) 70.05(3), Ni(1)−S(4)−Ni(2) 70.18(3).

2-SH)]$^{2-}$ (one phosphine, one terminal thiolate, and two bridging thiolates) coordinated to each Ni(II) center and the acute dihedral angles (Ni(1)S(1)S(2) and Ni(2)S(1)S(2)).

As shown in part b of Scheme 3, upon injecting O_2 (3 mL, 14 psi, at 290 K) into a THF solution of **4** (0.126 g, 0.1 mmol) at ambient temperature, the reaction ensued over 2 h to give dark-green, thermally stable dinuclear Ni(III) [Ni^{III}-(P(*o*-C_6H_3-3-$SiMe_3$-2-S)$_2$(*o*-C_6H_3-3-$SiMe_3$-2-μ-S))]$_2$ (**5**) characterized by single-crystal X-ray diffraction and UV−vis spectroscopy, and byproduct H_2O identified ^{1}H NMR.[11] The ^{1}H NMR spectrum of **5** in CD_2Cl_2 exhibits the signals for the trimethylsilyl protons at δ 0.49 (s), 0.23 (s), −0.59 (s), and the expected signals for the benzene protons at 6.85 (t), 6.89 (t), 7.33 (dd), 7.39 (t), 7.41 (t), 7.81 (dd), 8.12 (d). **5** in frozen CH_2Cl_2 shows EPR silent at 77 K. On the basis of ^{1}H NMR, EPR, and magnetic measurements, **5** was characterized as a diamagnetic species. Thus, the electronic structure of **5** can be best described as two paramagnetic d^7 Ni^{III} cores with antiferromagnetic coupling ($J = -3.13$ cm^{-1}), that is, both centers have $S = {}^1/_2$ spins magnetically coupled to each other possibly via the direct d−d orbital overlap (Ni-(1)···Ni(2) = 2.6026(7) Å) and the bridging sulfurs. Both complexes show the butterfly structure of the Ni(μ-S)$_2$Ni unit on going from Ni(II) **4** to Ni(III) **5** with little Ni−S−Ni bond angles and a Ni···Ni distance change (Ni−S−Ni bond angles of 70.59(4) and 70.33(4)° and a Ni···Ni distance of 2.5808-(8) Å for **4**, and 70.05(3) and 70.18(3)°, and 2.6026(7) Å for **5**). Figure 6 displays a thermal ellipsoid plot of **5** containing 0.5 THF solvent in crystal lattice, and selected bond distances and angles are given in the figure caption. Analysis of the bond angles of **5** reveals that Ni(1) and Ni-(2) are best described as existing in a distorted geometry midway between trigonal bipyramidal and tetragonal pyramidal. The mean Ni−$S_{(bridging)}$/Ni−$S_{(terminal)}$ lengths of 2.268-(1)/2.243(1) Å observed in **5** are longer than those of 2.239(1) and 2.156(1) Å found in **4**, respectively. The lengthening of the average Ni−S bonds of **5** can be ascribed to the strain effect of the chelating ligands in the coordination sphere from tridentate to tetradentate, which overwhelms the contracting effect caused by the metal-centered oxidation.

The electrochemistry of **5**, measured in THF with 0.1 M [*n*-Bu_4N][PF_6] supporting electrolyte at ambient temperature (scan rate 100 mV/s), reveals two reversible oxidation−reduction processes at −0.775 and −1.492 V ($E_{1/2}$) (vs Cp_2-Fe/Cp_2Fe^+), respectively (Figure 7). For $E_{1/2} = -0.775$ V, **5** undergoes one-electron reduction ($\Delta E_p = 167$ mV, $i_{pa}/i_{pc} = 0.59$) to a mixed-valence [Ni(III)Ni(II)] species, which can be further reduced to a [Ni(II)Ni(II)] species at $E_{1/2} = -1.492$ V ($\Delta E_p = 222$ mV, $i_{pa}/i_{pc} = 0.84$). It is noticed that the value of i_{pa}/i_{pc} at −0.775 V ($E_{1/2}$ value of the Ni^{3+}−Ni^{3+}/Ni^{3+}−Ni^{2+} couple) is dramatically different from the value of 1. However, when the scan range (potential) was switched from 0.0 to −1.0 V, the value of i_{pa}/i_{pc} at −0.775 V is close to 1 (0.83) and the value of i_{pc} at −0.389 V becomes smaller. These results may implicate that the mixed-valence [Ni(III)−Ni(II)] complex is unstable.

Mixed-Valence [Ni(II)−Ni(III)] [Na-18-crown-6-ether]-[Ni_2(P(*o*-C_6H_3-3- $SiMe_3$-2-S)$_3$)$_2$] (6), [Ni_2(P(*o*-C_6H_3-3-$SiMe_3$-2-S)$_3$)(P(*o*-C_6H_3-3-$SiMe_3$-2-S)$_2$(*o*-C_6H_3− 3-$SiMe_3$-2-SCH_3))] (7) and [Ni(II)−Ni(II)] [K-18-crown-6-ether]$_2$[Ni_2(P(*o*-C_6H_3-3- $SiMe_3$-2-S)$_3$)$_2$] (8). When a THF solution of **5**, [Na]-

(13) (a) Barclay, G. A.; McPartlin, E. M.; Stephenson, N. C. *Acta Crystallogr.* **1969**, *B25*, 1262−1273. (b) Nicholson, J. R.; Christou, G.; Huffman, J. C.; Folting, K. *Polyhedron* **1987**, *6*, 863−870. (c) Snyder, B. S.; Rao, Ch. P.; Holm, R. H. *Aust. J. Chem.* **1986**, *39*, 963−974. (d) Villa, A. C.; Manfredotti, A. G.; Nardelli. M.; Pelizzi, C. *Chem. Commun.* **1970**, 1322−1323. (e) Fackler, J. P., Jr.; Zegarski, W. J. *J. Am. Chem. Soc.* **1973**, *95*, 8566−8574. (f) Schwarzenbach, G. *Chem. Zvesti* **1965**, *19*, 200−208. (g) Vance, T. B., Jr.; Warner, L. G.; Seff, K. *Inorg. Chem.* **1977**, *16*, 2106−2110. (h) Handa, M.; Mikuriya, M.; Okawa, H.; Kida, S. *Chem. Lett.* **1988**, 1555−1558. (i) Colpas, G. J.; Kumar, M.; Day, R. O.; Maroney, M. J. *Inorg. Chem.* **1990**, *29*, 4779−4788. (j) Watson, A. D.; Rao, Ch. P.; Dorfman, J. R.; Holm, R. H. *Inorg. Chem.* **1985**, *24*, 2820−2826. (k) Allan, C. B.; Davidson, G.; Choudhury, S. B.; Gu, Z.; Bose, K.; Day, R. O.; Maroney, M. J. *Inorg. Chem.* **1998**, *37*, 4166−4167. (l) Choudhury, S. B.; Pressler, M. A.; Mirza, S. A.; Day, R. O.; Maroney, M. J. *Inorg. Chem.* **1994**, *33*, 4831−4839.

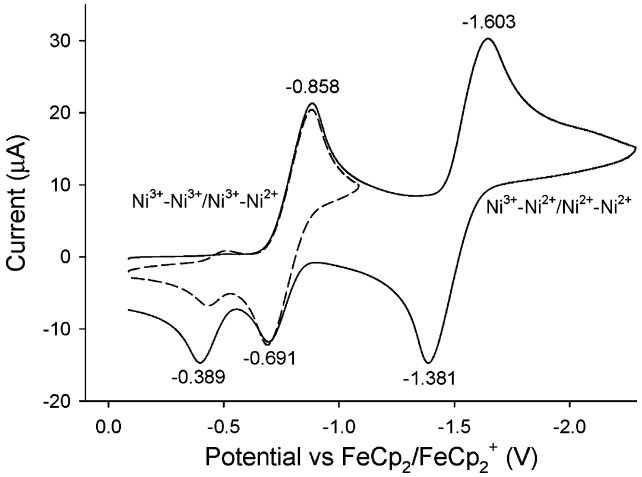

Figure 7. Cyclic voltammograms of **5** in the scan range (a) 0 to −2.5 V (solid line) and (b) 0 to −1.0 V (dash line). The rest potential was measured at −0.47 V.

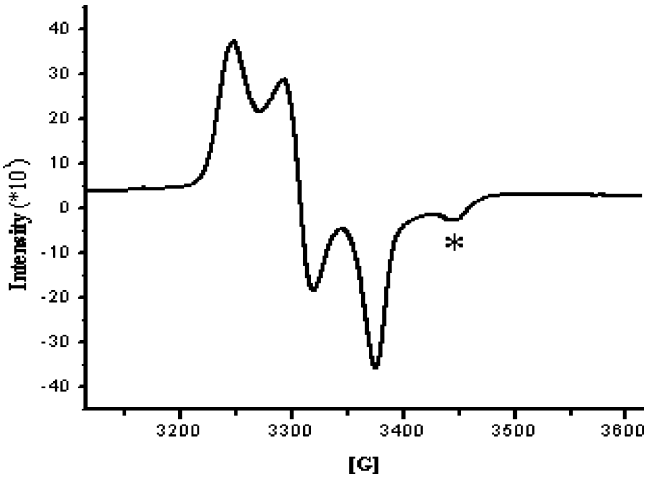

Figure 8. EPR spectrum of **6** with *g* values of 2.11, 2.07, and 2.03 at 77 K (* = impurity) (an isotropic signal with *g* values of 2.077 at 298 K).

$[BEt_3H]$ (or KC_8), and 18-crown-6-ether (1:1:2 molar ratio) were stirred at ambient temperature for 1 h (part c of Scheme 3), a reduction occurred to yield the mixed-valence [Ni(II)−Ni(III)] [Na-18-crown-6-ether][Ni_2(P(*o*-C_6H_3-3-$SiMe_3$-2-$S)_3)_2$] (**6**), identified by UV−vis, EPR, and single-crystal X-ray diffraction. Compared to the rhombic signal with *g* values of 2.304, 2.091, and 2.00 (4.2 K) observed in complex [Ni^{III}(SePh)(P(*o*-C_6H_3-2-$S)_3$)]$^-$ (**11**), the 77 K EPR spectrum of **6** exhibits high rhombicities with three principal *g* values of 2.113, 2.073, and 2.033 (an isotropic signal with a *g* value of 2.077 at 298 K) (Figure 8).[14] The UV−vis spectrum of **6** exhibits an intense absorption around 1124 nm with an extinction coefficient of >2000 L mol^{-1} cm^{-1}, which may be ascribed to the intervalence transition of the fully delocalized mixed-valence complexes (Supporting Information Figure S1).[14] These results support that **6** adopts a fully delocalized mixed-valence [Ni(III)−Ni(II)] electronic configuration in a distorted-square-planar ligand field.

(14) (a) Stebler, A.; Ammeter, J. H.; Fuerholz, U.; Ludi, A. *Inorg. Chem.* **1984**, *23*, 2764−2767. (b) Ondrechan, M. J.; Ko, J.; Zhang, L.-T. *J. Am. Chem. Soc.* **1987**, *109*, 1672−1676.

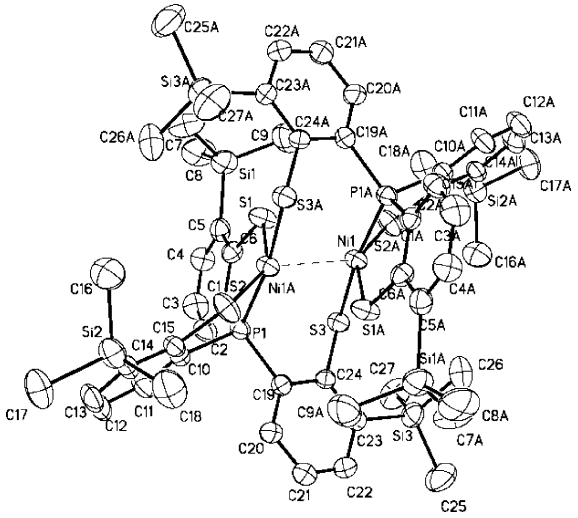

Figure 9. ORTEP drawing and labeling scheme of **6** with thermal ellipsoids drawn at 30% probability level. Selected bond distances (Å) and angles (°): Ni(1)−S(1A) 2.1540(17), Ni(1)−S(2A) 2.2118(15), Ni(1)−S(3) 2.2418(15), Ni(1)···S(1) 2.680(2), Ni(1)···S(3A) 3.905(2), Ni(1)−P(1A) 2.1546(15), Ni(1)···Ni(1A) 2.8290(13); P(1A)−Ni(1)−S(1A) 88.50(6), P(1A)−Ni(1)−S(2A) 86.27(6), S(1A)−Ni(1)−S(2A) 148.99(8), P(1A)−Ni(1)−S(3) 169.99(6), S(1A)−Ni(1)−S(3) 94.70(6), S(2A)−Ni(1)−S(3) 86.12(6), P(1A)−Ni(1)−S(1) 91.03(5), S(1A)−Ni(1)−S(1) 109.32(6), P(1A)−Ni(1)−Ni(1A) 89.83(5), S(1A)−Ni(1)−Ni(1A) 63.39(6), S(2A)−Ni(1)−Ni(1A) 146.99(7).

The single-crystal X-ray structure of **6** is depicted in Figure 9, and selected bond dimensions for **6** are presented in the figure caption. **6** consists of two four-coordinated nickel centers in a distorted-square-planar geometry, with three thiolate sulfur atoms and one phosphorus atom. The two nickel atoms and two sulfur atoms (S(1) and S(1A)) of **6** are almost constrained to a coplanar arrangement. Two groups, the coplanar [S(1A)Ni(1)Ni(1A)S(1)] and the coplanar [Ni(1)S(3)P(1)Ni(1A)S(3A)P(1A)], are in a perpendicular conformation with an angle of 89.82°. Compared to the bridging Ni(1)−S(1) and Ni(1)−S(4) bond distances of 2.253(1) and 2.284(1) Å, respectively, found in **5**, the longer Ni(1)···S(1) distance of 2.680(2) Å (Ni(1)···S(3A) 3.905(2) Å) observed in **6** indicates that reduction of **5** yielding **6** (reduction of [$Ni^{III}Ni^{III}$] to mixed-valence [$Ni^{III}Ni^{II}$]) results in the elongation of Ni(1)···S(1) distance and the relief of the strained tetradentate bonding mode. The geometrical rearrangement from the butterfly structure of [Ni(μ-$S)_2$Ni] unit of **5** to the diamond shape of [$Ni(S)_2$Ni] core of **6** reflects the effects caused by the addition of one electron. Upon one-electron reduction of **5** yielding **6**, the Ni···Ni distance is lengthened by as much as 0.22 Å. This result implicates, qualitatively, that the SOMO in **6** can be identified as having antibonding character in Ni···Ni interaction. Compared to the Ni···Ni distance of 2.6026(7)/2.501 Å and the ligation mode of the coordinated [P(*o*-C_6H_3-3-$SiMe_3$-2-$S)_3]^{3-}$/[P(*o*-C_6H_4-2-$S)_3]^{3-}$ ligands observed in **5** and [Ni(P(*o*-C_6H_4-2-$S)_2$(*o*-C_6H_4-2-μ-S))]$_2^-$ (**10**), respectively, the longer Ni···Ni distance (2.829(1) Å) and the ligation mode of the coordinated [P(*o*-C_6H_3-3-$SiMe_3$-2-$S)_3]^{3-}$ ligands of **6** are attributed to the more electron-rich functionalities of the mixed-valence [Ni(II)Ni(III)] core and the electronic/steric perturbations

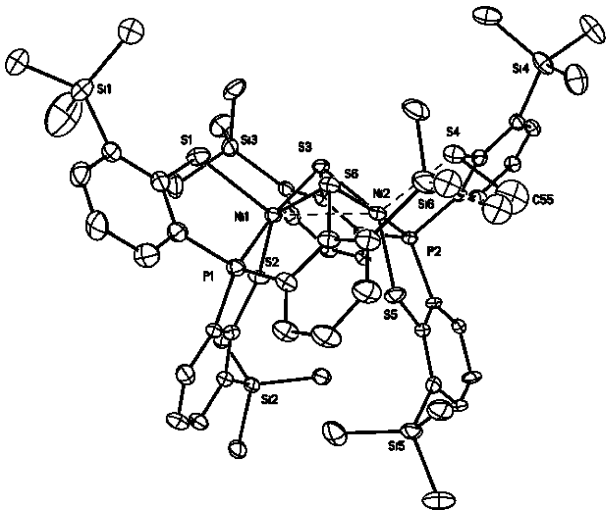

Figure 10. ORTEP drawing and labeling scheme of **7** with thermal ellipsoids drawn at 30% probability level. Selected bond distances (Å) and angles (°): Ni(1)−S(1) 2.3544(18), Ni(1)−S(2) 2.1885(15), Ni(1)−S(3) 2.2551(15), Ni(1)−S(6) 2.2699(16), Ni(1)−P(1) 2.1184(16), Ni(1)···Ni(2) 2.6088(11), Ni(2)−S(3) 2.2686(15), Ni(2)−S(4) 2.4036(18), Ni(2)−S(5) 2.1986(15), Ni(2)−S(6) 2.2600(16), Ni(2)−P(2) 2.1120(16); P(1)−Ni(1)−S(2) 86.95(6), P(1)−Ni(1)−S(3) 171.96(6), S(2)−Ni(1)−S(3) 94.48(6), P(1)−Ni(1)−S(6) 86.56(6), S(2)−Ni(1)−S(6) 145.32(6), S(3)−Ni(1)−S(6) 87.79(6), P(1)−Ni(1)−S(1) 87.84(6), S(2)−Ni(1)−S(1) 113.02(6), P(2)−Ni(2)−S(5) 87.50(6), P(2)−Ni(2)−S(6) 172.42(6), S(5)−Ni(2)−S(6) 95.01-(6), P(2)−Ni(2)−S(3) 86.08(6), S(5)−Ni(2)−S(3) 143.92(6), S(5)−Ni(2)−S(4) 112.02(6), Ni(1)−S(6)−Ni(2) 70.32(5), Ni(1)−S(3)−Ni(2) 70.44(5), Ni(2)−S(4)−C(55) 104.3(5).

from the substituted trimethylsilyl groups (the strongly σ-donating $SiMe_3$ group).

To further corroborate the electronic effect (oxidation states of nickel) modulating the Ni···Ni interaction of dinuclear **5** and **6**, the neutral dinuclear $[Ni_2(P(o\text{-}C_6H_3\text{-}3\text{-}SiMe_3\text{-}2\text{-}S)_3)(P(o\text{-}C_6H_3\text{-}3\text{-}SiMe_3\text{-}2\text{-}S)_2(o\text{-}C_6H_3\text{-}3\text{-}SiMe_3\text{-}2\text{-}SCH_3))]$ (**7**) was synthesized. As shown in part d of Scheme 3, treatment of **6** with $[Me_3O][BF_4]$ in THF−CH_3CN solution yielded **7**, identified by UV−vis and single-crystal X-ray diffraction. X-ray crystal structure of **7** is depicted in Figure 10, and selected bond coordinates are presented in the figure captions. The apparently shorter Ni(1)···Ni(2) distance (2.6088(11) Å) of **7**, compared to the Ni···Ni distance of 2.829(1) Å in **6**, indicates a greater extent of Ni(1)···Ni(2) interaction in **7**. Obviously, the electronic perturbation caused by the sulfur methylation of **6** triggers the stronger Ni(1)···Ni(2) interaction accompanied by the geometrical rearrangement from the diamond shape of the $[Ni(S)_2Ni]$ core of **6** to the butterfly structure of the $[Ni(\mu\text{-}S)_2Ni]$ unit of **7** to reimburse the deficiency of electron density surrounding [Ni(II)Ni(III)] centers. **7** exhibited the disorder of S(1) and S(4) atoms. The combined scattering factors, $0.65S(1)_{(thiolate)} + 0.35S(1)_{(thioether)}$ and $0.35S(4)_{(thiolate)} + 0.65S(4)_{(thioether)}$, respectively, were used in the refinement. There is weak interaction between Ni(1)/Ni(2) and the thioether sulfur atom (Ni(1)···S(1) distance of 2.354(2) and Ni(2)···S(4) distance of 2.404(2) Å). Interestingly, the frozen-solution EPR spectrum of **7** (77 K) in diethyl ether (Figure 11), essentially indistinguishable from those of the 77 K EPR spectrum of the fully delocalized mixed-valence **6**, exhibits high rhombicities with three principal g values of 2.17, 2.05, and 2.02,

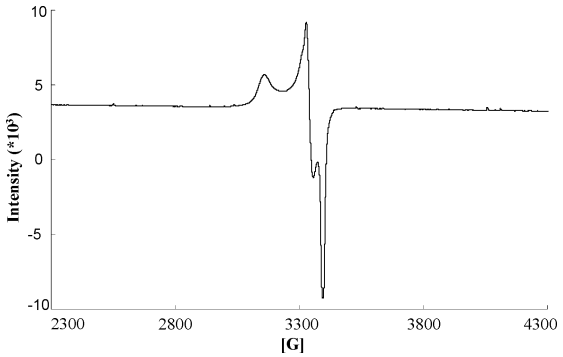

Figure 11. X-band frozen solution EPR spectrum of **7** with g values of 2.17, 2.05, and 2.02, recorded at 77 K (an isotropic signal with g value of 2.08 at 298 K).

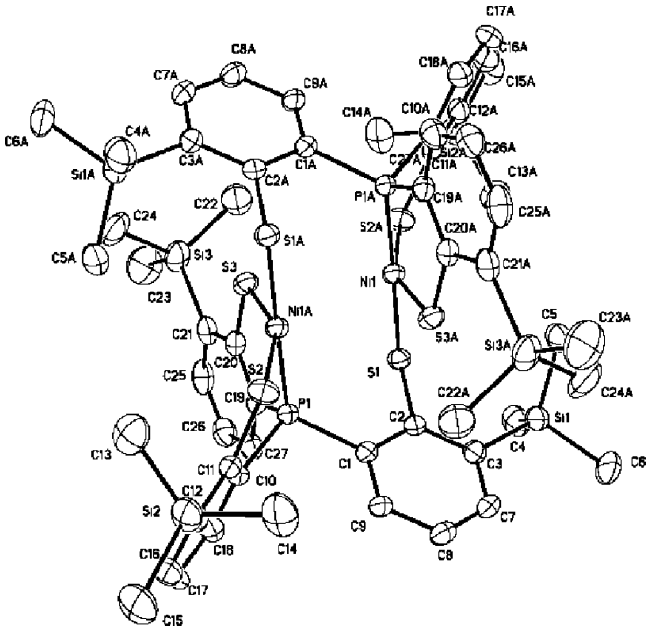

Figure 12. ORTEP drawing and labeling scheme of **8** with thermal ellipsoids drawn at 30% probability level. Selected bond distances (Å) and angles (°): Ni(1)−P(1A) 2.1097(14), Ni(1)−S(1) 2.2377(14), Ni(1)−S(2A) 2.2171(16), Ni(1)−S(3A) 2.1678(15), Ni(1)···S(3) 3.146, Ni(1)···Ni(1A) 3.186; P(1A)−Ni(1)−S(3A) 88.78(6), P(1A)−Ni(1)−S(2A) 86.62(6), S(3A)−Ni(1)−S(2A) 154.26(7), P(1A)−Ni(1)−S(1) 175.87(6), S(3A)−Ni(1)−S(1) 95.35(6), S(2A)−Ni(1)−S(1) 89.58(6).

which are different from those of the mononuclear d^7 Ni-(III) complex $[Ni^{III}(SePh)(P(o\text{-}C_6H_4S)_3)]^-$.[11a,11c] These results implicate that **7** may exist as the delocalized mixed-valence [Ni(II)−Ni(III)] complex, owing to the strong interaction between the nickel centers and between nickel and sulfur,[14] although the valence-trapped case cannot be unambiguously excluded from this result alone.

Therefore, the lengthening of the Ni···Ni distance was expected to be driven by reduction of **6**; the reduction of **6** by 1 equiv of KC_8 in THF under N_2 at ambient temperature yielded a dianionic $[Ni_2(P(o\text{-}C_6H_3\text{-}3\text{-}SiMe_3\text{-}2\text{-}S)_3)_2]^{2-}$ (**8**) with a Ni···Ni distance of 3.186 Å (part e of Scheme 3). Figure 12 displays the ORTEP plot of **8**. The nickel center is best described as existing in a distorted-square-planar coordination environment surrounded by three thiolate sulfur atoms and one phosphorus atom. In comparison with the butterfly structure of the $[Ni(\mu\text{-}S)_2Ni]$ core of **4** with a Ni(1)···Ni(2) distance of 2.5808(8) Å, the two coplanar $[NiS_3P]$

([Ni(1)S(1)S(3A)S(2A)P(1A)] and [Ni(1A)S(1A)S(3)S(2)P(1)]) with an Ni···Ni distance of 3.186 Å in **8** are almost parallel. The longer Ni···Ni distance, compared to that of **4**, is presumably ascribed to the more electron-rich [Ni(II)Ni(II)] centers of **8**, deriving from the stronger electron-donating thiolate-coordinated ligands.

Conclusion and Comments

Studies on the mononuclear/dinuclear Ni(III)-/Ni(II)-thiolate **1**−**5**, **8**, and the mixed-valence [Ni(II)−Ni(III)] thiolate complexes **6**−**7** have led to the following results, including certain results from earlier studies.

(1) In **3b**, the presence of intramolecular [Ni···H−S] interaction was verified in the solid state by the observation of a lower IR ν_{S-H} stretching frequency compared to those of **1a** and **3a** and subsequently was confirmed by single-crystal X-ray diffraction, respectively. The pendant thiol interaction modes ([Ni···H−S] vs [Ni−S···H−S]) in the solid state (**1a**/**3a** vs **3b**) are controlled by the solvent pairs of crystallization. Obviously, the results obtained from this work show that the IR ν_{S-H} stretching frequency in combination with the torsion angle ∠Ni−P(1)−C(14)−C(13) may serve as an efficient tool for the discrimination of the existence of the intramolecular [Ni···H−S]/[Ni−S···H−S] interactions in complexes $[Ni^{II}(L)(P(o\text{-}C_6H_3\text{-}3\text{-}SiMe_3\text{-}2\text{-}S)_2(o\text{-}C_6H_3\text{-}3\text{-}SiMe_3\text{-}2\text{-}SH))]^-$ (L = SePh, Cl).

(2) In contrast to **1a** and **3a**/**3b**, neutral dinuclear complex **4** containing the less-basic nickel center (the less electronic density) regulated by the coordinated ligands does not show the intramolecular [Ni···H−S]/[Ni−S···H−S] interactions.

(3) Oxidation of dinuclear complex **4** by O_2 yielded stable dinuclear complex **5** with a Ni···Ni distance of 2.6026(7) Å. From the viewpoint of the absence of paramagnetism (SQUID) and the EPR signal, **5** can be considered as d^7 Ni(III) and d^7 Ni(III) units antiferromagnetically coupled to each other (J value of -3.13 cm^{-1} in **5**), where thiolate bridges may also mediate the antiferromagnetic interactions. The electrochemistry of **5** exhibits two reversible oxidation−reduction processes at −0.775 and −1.492 V ($E_{1/2}$) (vs Cp_2Fe/Cp_2Fe^+), respectively.

(4) The reduction of **5** yielded the mixed-valence [Ni(II)−Ni(III)] complex $[Ni_2(P(o\text{-}C_6H_3\text{-}3\text{-}SiMe_3\text{-}2\text{-}S)_3)_2]^-$ (**6**), exhibiting an intense absorption band at 1124 nm, ascribed to the intervalence transition of the fully delocalized mixed-valence complexes. Rhombic EPR signals ($g_1 = 2.11$, $g_2 = 2.07$, and $g_3 = 2.03$ at 77 K) confirmed the existence of the unpaired electron in **6**.

(5) As shown in Scheme 4, the geometrical (coordination environment) change from distorted square pyramidal to distorted square planar (i.e., from butterfly structure of the [Ni(μ-S)$_2$Ni] core to the diamond shape of the [NiS$_2$Ni] core) occurs upon going from a [d^7 Ni(III)−d^7 Ni(III)] electronic structure of **5** to a fully delocalized mixed-valence [d^8 Ni(II)-d^7 Ni(III)] electronic structure of **6**. In particular, the different oxidation levels of the [PS$_3$Ni−NiPS$_3$] units between **5** and **6** reflect the distinctly different Ni···Ni distances, 2.6026(7) for **5** and 2.8290(13) Å for **6**, to reach the optimum electron density of the [PS$_3$Ni−NiPS$_3$] core of **5** and **6**. The electronic perturbation from the sulfur methylation of **6** triggers the stronger Ni···Ni interaction and the geometrical rearrangement from the diamond shape of the [NiS$_2$Ni] core to the butterfly structure of [Ni(μ-S)$_2$Ni], resulting in the formation of **7** (Scheme 4). Presumably, the shortening of the Ni···Ni distance of **7** (vs **6**) was employed to reimburse the electron deficiency induced by methylation, neutralizing the thiolate negative charge. Also, the geometrical change of the nickel centers from distorted tetrahedral to square planar and the lengthening of the Ni···Ni distance (from 2.581 to 3.186 Å) occur upon going from a neutral [Ni(II)Ni(II)] electronic structure of **4** to a dianionic [Ni(II)Ni(II)] electronic structure of **8**. Such geometrical differences as determined by the nickel oxidation state in **5** versus that in **6** and determined by the coordinated ligands in **6** versus those in **7** (or in **4** versus those in **8**) demand ligands capable of matching the geometrical requirement of the [Ni(SR)$_2$Ni] unit as well as maintaining the preferred coordination number of the nickels (Scheme 4). Obviously, the presence/absence of Ni···Ni interaction in cooperation with the geometrical rearrangement was employed by dinuclear complexes **4**−**8** as an efficient tool to reach an optimum electronic condition to stabilize the dinuclear complexes.

Scheme 4

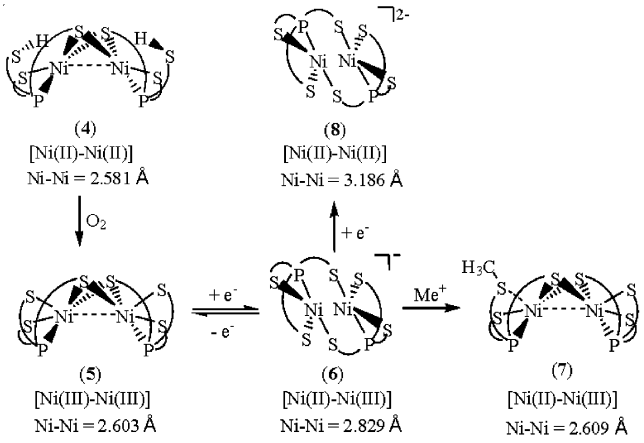

These results unambiguously illustrate the aspects of how a coordinated ligand and the electronic states (oxidation states) of two nickel centers function to trigger the geometrical rearrangement, to promote the stability of the dinuclear nickel complexes via the Ni···Ni interaction. This result may provide some clues to rationalize the oxidized-form active-site structure of [NiFe] hydrogenases, a heterobimetallic $(S_{cys})_2Ni(\mu\text{-}S_{cys})_2(\mu\text{-}X)Fe(CO)(CN)_2$ (X = O^{2-}, HO_2^-, OH^-) with the butterfly structure of the [Ni(μ-S$_{cys}$)$_2$-Fe] core and a Ni···Fe distance of 2.6 Å.

Experimental Section

Manipulations, reactions, and transfers were conducted under nitrogen according to Schlenk techniques or in a glovebox. Solvents were distilled under nitrogen from appropriate drying agents (diethyl ether from CaH_2; acetonitrile from $CaH_2-P_2O_5$; methylene chloride from CaH_2; hexane and tetrahydrofuran (THF) from sodium benzophenone) and stored in dried, N_2-filled flasks over 4 Å molecular sieves. Nitrogen was purged through these solvents before

use. Solvent was transferred to the reaction vessel via a stainless cannula under a positive pressure of N_2. The reagents bis(triphenylphosphoranylidene)ammonium chloride ([PPN][Cl]) (Fluka), diphenyl diselenide, nickel(II) dichloride, Deuterium oxide, 99.9 atom % D (Aldrich) were used as received. Compounds [P(*o*-C_6H_3-3-$SiMe_3$-2-SH)$_3$],[15] [PPN][Ni(CO)(SePh)$_3$], and [PPN][Ni(SePh)-(P(*o*-C_6H_3-3-$SiMe_3$-2-S)$_3$)] were synthesized by published procedures.[11,16] Infrared spectra of the ν(S−H) stretching frequencies were recorded on a PerkinElmer model spectrum one B spectrophotometer with sealed solution cells (0.1 mm, KBr windows) or KBr solid. UV−vis spectra were recorded on a GBC Cintra 10e. ^{1}H and ^{2}H NMR spectra were obtained on a Varian Unity-500 spectrometer. Electrochemical measurements were performed with a CHI model 421 potentionstat (CH Instrument) instrumentation. Cyclic voltammograms were obtained from 2.0 mM analyte concentration in THF using 0.1 M [*n*-Bu_4N][PF_6] as a supporting electrolyte. Potentials were measured at 298 K versus a Ag/AgCl reference electrode using a glassy-carbon working electrode. Under the conditions employed, the potential (*V*) of the ferrocinium/ferrocene couple was 0.39 (CH_2Cl_2). Analyses of carbon, hydrogen, and nitrogen were obtained with a CHN analyzer (Heraeus).

Preparation of [PPN][Ni(SePh)(P(*o*-C_6H_3-3-$SiMe_3$-2-S)$_2$(*o*-C_6H_3-3-$SiMe_3$-2- SH))] (1a) and (1b). Complexes [PPN][Ni(CO)-(SePh)$_3$] (0.2 mmol, 0.218 g)[16] and P(C_6H_3-3-$SiMe_3$-2-SH)$_3$ (0.2 mmol, 0.115 g) were loaded into a 50-mL flask and 15 mL of THF was added by a cannula under positive N_2 pressure. The reaction mixture was stirred at ambient temperature for 1 h, and then hexane (20 mL) was added to precipitate the red-brown solid [PPN][Ni-(SePh)(P(*o*-C_6H_3-3-$SiMe_3$-2-S)$_2$(*o*-C_6H_3-3- $SiMe_3$-2-SH))] (**1**) (0.225 g, 85%). Diffusion of diethyl ether into a THF solution of **1** at room temperature for 1 week yielded layered brown-red crystals characterized as **1a** (0.212 g, 80%) (Scheme 1). IR: 2250 w (ν_{S-H}) cm^{-1} (KBr). ^{1}H NMR (C_4D_8O): δ 8.59 (br) (SH), 6.65∼6.77 (m), 6.87 (t), 7.15∼7.33 (m) (PhSe, P(*o*-C_6H_3-3-$SiMe_3$-2-S)$_3$), 0.20 (s), 0.30 (s) ($SiMe_3$). However, diffusion of hexane into a THF solution of **1** at ambient temperature for 1 week yielded chunky dark red-brown crystals characterized as **1b** (0.220 g, 83%) (Scheme 1) suitable for X-ray crystallography. IR: 2137 w (ν_{S-H}) cm^{-1} (KBr). ^{1}H NMR (C_4D_8O): δ 8.59 (br), 6.65∼6.77 (m), 6.87 (t), 7.15∼7.33 (m) (PhSe, P(*o*-C_6H_3-3-$SiMe_3$-2-S)$_3$), 0.20 (s), 0.30 (s) ($SiMe_3$). Absorption spectrum (THF) [λ_{max}, nm (ϵ, M^{-1} cm^{-1})]: 420 (2700), 500 (1150). Anal. Calcd for $C_{69}H_{72}NNiP_3S_3SeSi_3$: C, 62.48; H, 5.47; N, 1.06. Found: C, 62.18; H, 5.22; N, 0.98.

Preparation of [PPN][Ni(Cl)(P(*o*-C_6H_3-3-$SiMe_3$-2-S)$_2$(*o*-C_6H_3-3-$SiMe_3$-2- SH))] (3a) and (3b). Compound P(C_6H_3-3-$SiMe_3$-2-SH)$_3$ (0.058 g, 0.1 mmol) and [PPN]$_2$[$NiCl_4$] (0.128 g, 0.1 mmol), prepared from reaction of $NiCl_2$ (0.1 mmol) and [PPN][Cl] (0.2 mmol) in MeOH, were dissolved in mixed solvent THF−CH_3CN (10:1 volume ratio). After the reaction mixture was stirred at ambient temperature for 30 min, hexane was added to separate the red-brown precipitate and the orange-red solution. The orange-red solution was then transferred to another flask under positive N_2, and dried under a vacuum to obtain the orange-red solid characterized as complex [Ni(P(*o*-C_6H_3-3-$SiMe_3$-2-S)$_2$(*o*-C_6H_3-3-$SiMe_3$-2-SH))]$_2$ (**4**) (0.032 g, 25%). The red-brown solid was then redissolved in THF (5 mL) and filtered through Celite to remove [PPN][Cl]. Hexane was then added to precipitate the red-brown solid characterized as complex [PPN][Ni(Cl)(P(*o*-C_6H_3-3-$SiMe_3$-2-S)$_2$(C_6H_3-3-$SiMe_3$-2-SH))] (**3**) (0.072 g, 65%). Diffusion of diethyl ether into a CH_2Cl_2 solution of **3** at −15 °C for 4 weeks led to layered red-brown crystals of **3a** (0.04 g, 33%) (Scheme 2). IR: 2287 w (ν_{S-H}) cm^{-1} (KBr, pellet). ^{1}H NMR (C_4D_8O): δ 8.54 (br) (SH), 6.73∼6.74 (m), 6.87 (t), 7.17∼7.38 (m) (P(C_6H_3-3-$SiMe_3$-2-S)$_3$), 0.29 (s) ($SiMe_3$) ppm. On the other hand, diffusion of hexane into a CH_2-Cl_2 solution of **3** at −15 °C for 4 weeks yielded chunky dark red-brown crystals of **3b** (0.041 g, 33%) (Scheme 2) suitable for X-ray crystallography. IR: 2235 w (ν_{S-H}) cm^{-1} (KBr). ^{1}H NMR (C_4D_8O): δ 8.54 (br) (SH), 6.73∼6.74 (m), 6.87 (t), 7.17∼7.38 (m) (P(C_6H_3-3-$SiMe_3$-2-S)$_3$); 0.29 (s) ($SiMe_3$). Absorption spectrum (CH_2Cl_2) [λ_{max}, nm (ϵ, M^{-1} cm^{-1})]: 430 (2200), 530 (1200). Anal. Calcd for $C_{63}H_{67}ClNiNP_3S_3Si_3$: C, 62.76; H, 5.60; N, 1.16. Found: C, 62.86; H, 5.89, N, 1.24.

Preparation of [Ni(P(*o*-C_6H_3-3-$SiMe_3$-2-S)$_2$(*o*-C_6H_3-3-$SiMe_3$-2-SH))]$_2$ (4). A portion (0.12 mL) of [Et_3O][BF_4] was slowly added into a THF (10 mL) solution of **1** (0.133 g, 0.1 mmol) at 5 °C. A vigorous reaction occurred with the white precipitate [PPN][BF_4]. Hexane (10 mL) was added, and the resulting mixture was filtered through Celite to remove the insoluble [PPN][BF_4]. Solvent was removed under a vacuum to yield complex [Ni(P(*o*-C_6H_3-3-$SiMe_3$-2-S)$_2$(*o*-C_6H_3-3-$SiMe_3$− 2-SH))]$_2$ (**4**) (0.088 g, 70%). Hexane (3 mL) was added to redissolve **4** and recrystallization from hexane solution at −15 °C for 4 weeks gave red-brown crystals suitable for X-ray crystallography. IR: 2385 w (ν_{S-H}) cm^{-1} (KBr, pellet). ^{1}H NMR ($CDCl_3$): δ 6.24 (d) (SH), 6.39 (t), 6.83 (t), 6.91 (t), 7.15 (t), 7.25 (t), 7.42 (d), 7.64 (d) (P(C_6H_3-3-$SiMe_3$-2-S)$_3$), −0.11 (s), 0.33 (s), 0.51 (s) ($SiMe_3$). Absorption spectrum (THF) [λ_{max}, nm ϵ, M^{-1} cm^{-1})]: 440 (3080), 5350 (1050). Anal. Calcd for $C_{54}H_{74}Ni_2P_2S_6Si_6$: C, 51.34; H, 5.90. Found: C, 50.93; H, 6.33.

D/H Exchange for the Reaction of 4 and D_2O. To a THF (10 mL) solution of **4** (0.126 g, 0.1 mmol) at 5 °C, a 100-fold excess of D_2O (0.18 mL, 10 mmol) was added. The reaction solution containing the mixture solution of **4** and D_2O was stirred for 24 h at 5 °C. Solvent was removed under a vacuum and hexane (5 mL) was added to redissolve the red-brown solid. The flask containing the red-brown solution was tightly sealed and kept at −15 °C for 4 weeks. The crystals [Ni(P(*o*-C_6H_3-3-$SiMe_3$-2-S)$_2$(*o*-C_6H_3-3-$SiMe_3$-2-SD))]$_2$ (**4-D**) and **4** were isolated. IR (KBr, pellet): 1748 (ν_{S-D}) cm^{-1}. ^{2}H NMR (C_4H_8O): δ 6.37 (br) (SD) versus C_4D_8O (natural abundance of D in C_4H_8O solvent, δ 1.73 and 3.58).

Preparation of [Ni(P(*o*-C_6H_3-3-$SiMe_3$-2-S)$_3$)]$_2$ (5). Pure oxygen gas (3 mL, 14 psi, at 290 K) was injected through a red-brown hexane solution (10 mL) of **4** (0.126 g, 0.1 mmol) at room temperature. A significant change in color from red brown to dark green occurred after the reaction mixture was stirred for an additional 2 h at room temperature. The resulting solution was filtered, and then the solution was concentrated to 3 mL under a vacuum. Crystallization from hexane solution of complex [Ni(P(*o*-C_6H_3-3-$SiMe_3$-2-S)$_3$)]$_2$ (**5**) (0.076 g, 60%) at −15 °C for 4 weeks led to dark-green crystals suitable for X-ray crystallography. ^{1}H NMR (CD_2Cl_2): δ 6.85 (t), 6.89 (t), 7.33 (d), 7.39 (t), 7.41(t), 7.81 (dd), 8.12 (d) (P(*o*-C_6H_3-3-$SiMe_3$-2-S)$_3$), −0.59 (s), 0.23 (s), 0.49 (s) ($SiMe_3$). Absorption spectrum (CH_3CN) [λ_{max}, nm (ϵ, M^{-1} cm^{-1})]: 435 (5100), 636 (1750), 758 (550), 1154 (1300). FAB-mass spectrum: *m*/*z* 1260 (([NiP(*o*-C_6H_3-3-$SiMe_3$-2-S)$_3$]$_2$)$^+$, 40.6%); *m*/*z* 73 (($SiMe_3$)$^+$, 100%). Anal. Calcd for $C_{54}H_{72}Ni_2P_2S_6Si_6$: C, 51.42; H, 5.75. Found: C, 51.38; H, 5.90.

Preparation of [Na-18-crown-6-ether][Ni$_2$(P(*o*-C_6H_3-3-$SiMe_3$-2-S)$_3$)$_2$] (6). A 0.126 g of **5** (0.1 mmol) and 0.053 g of 18-crown-6-ether (0.2 mmol) were dissolved in 5 mL THF in a 30 mL Schlenk tube under nitrogen. A portion (0.1 mL) of $NaBEt_3H$ (0.1 M in THF solution) was then added into the Schlenk tube by syringe. The reaction solution was stirred under nitrogen at ambient

(15) Block, E.; Ofori-Okai, G.; Zubieta, J. *J. Am. Chem. Soc.* **1989**, *111*, 2327−2329.
(16) Liaw, W.-F.; Horng, Y.-C.; Ou, D.-S.; Chiang, C.-Y.; Lee, G.-H.; Peng, S.-M. *J. Am. Chem. Soc.* **1997**, *119*, 9299−9300.

temperature for 1 h and monitored by UV−vis. The color of the reaction solution changes from green to brown green. Hexane (20 mL) was then added to precipitate the brown-green solid [Na-18-crown-6-ether][Ni_2(P(*o*-C_6H_3-3-$SiMe_3$-2-S)$_3$)$_2$] (**6**) (yield 0.115 g, 65%). Crystals for X-ray diffraction analysis were obtained by a layer of hexane and THF solution of **6** at −20 °C. Absorption spectrum (THF) [λ_{max}, nm (ϵ, $M^{-1}cm^{-1}$)]: 654 (3667), 1142 (2548). Anal. Calcd for $C_{66}H_{96}P_2NaNi_2O_6S_6Si_6$: C, 51.19; H, 6.25. Found: C, 51.64; H, 6.48.

A THF solution (10 mL) of **5** (0.126 g, 0.1 mmol) was added to KC_8 solid (0.014 g, 0.1 mmol) in a 30 mL Schlenk tube under positive nitrogen. The reaction solution was stirred under nitrogen at ambient temperature for 1 h. The color of the reaction solution changed from green to brown green. Then a THF solution (5 mL) of 18-crown-6-ether (0.053 g, 0.2 mmol) was transferred to the above brown-green solution by cannula. After the reaction solution was stirred for another 3 h under nitrogen at ambient temperature, the brown-green solution was filtered through Celite to remove graphite and was monitored by UV−vis. The volume of solution was reduced to 5 mL under a vacuum, and then hexane (25 mL) was added to precipitate the brown-green solid [K-18-crown-6-ether][Ni_2(P(*o*-C_6H_3-3-$SiMe_3$-2- S)$_3$)$_2$] (**6′**) (yield 0.102 g, 65%) characterized by UV−vis and single-crystal X-ray diffraction.

Preparation of [Ni_2(P(*o*-C_6H_3-3-$SiMe_3$-2-S)$_3$)(P(*o*-C_6H_3-3-$SiMe_3$-2-S)$_2$(*o*-C_6H_3-3-$SiMe_3$-2-SCH_3))] (7). A CH_3CN solution (3 mL) of [Me_3O][BF_4] (0.015 g, 0.1 mmol) was added dropwise into the THF−CH_3CN (3:1 volume ratio) mixed solution of complex **6′** (0.156 g, 0.1 mmol) at 5 °C under N_2 atmosphere. The mixture solution was stirred for 30 min, then allowed to warm to room temperature, and stirred for another 2 h. The color of reaction solution changed from brown green to green. The mixture solution was dried under a vacuum and then redissolved in hexane. The green solution was filtered through Celite to remove the insoluble [K-18-crown-6-ether][BF_4]. Solvent was removed under a vacuum to yield [Ni_2(P(*o*-C_6H_3-3-$SiMe_3$-2-S)$_3$)(P(*o*-C_6H_3-3-$SiMe_3$-2-S)$_2$(*o*-C_6H_3-3-$SiMe_3$-2-SCH_3))] (**7**) (yield 0.091 g, 71%). A hexane solution of **7** kept at −15 °C for 4 weeks gave dark-green crystals suitable for X-ray crystallography. Absorption spectrum ($(Et)_2O$) [λ_{max}, nm (ϵ, M^{-1} cm^{-1})]: 421 (10 100), 495 (5456), 669 (3170), 1144 (2032). $C_{55}H_{75}Ni_2P_2S_6Si_6$: C, 51.75; H, 5.92. Found: C, 51.84; H, 6.17.

Preparation of [K-18-crown-6-ether]$_2$[Ni_2(P(*o*-C_6H_3-3-$SiMe_3$-2-S)$_3$)$_2$] (8). A THF solution (10 mL) of **6′** (0.155 g, 0.1 mmol) was added to KC_8 solid (0.014 g, 0.1 mmol) in a 30 mL Schlenk tube under positive nitrogen. The reaction solution was stirred under nitrogen at ambient temperature for 1 h. A color change of the reaction solution from brown green to red brown was observed. A THF solution (5 mL) of 18-crown-6-ether (0.053 g, 0.2 mmol) was then added to the above red-brown solution by cannula under positive nitrogen and stirred for another 3 h. The solution was then filtered through Celite to remove graphite. The volume of the solution was reduced to 5 mL under a vacuum, and hexane (25 mL) was added to precipitate the red-brown solid [K-18-crown-6-ether]$_2$[Ni_2(P(*o*-C_6H_3-3-$SiMe_3$-2-S)$_3$)$_2$] (**8**) (yield 0.125 g, 67%). Crystals suitable for X-ray diffraction were obtained by a layer of hexane and THF−CH_3CN (10:1 volume ratio) solution of **8** at −15 °C for 2 weeks.

Crystallography. Crystallographic data of **1a**/**1b**, **3a**/**3b**, **4**−**5**, **6**−**7**, and **8** were summarized in Supporting Information Tables S1−S5, respectively. Each crystal was mounted on a glass fiber and quickly coated in epoxy resin. Unit-cell parameters were obtained by least-squares refinement. Diffraction measurements for **1a**, **1b**, **3a**, **3b**, and **4**−**8** were carried out on a SMART CCD (Nonius Kappa CCD) diffractometer with graphite-monochromated Mo Kα radiation (λ = 0.7107 Å). **7** exhibited a disorder of the S(1) and S(4) atoms. The combined scattering factors, 0.65S(1)$_{(thiolate)}$ + 0.35S(1)$_{(thioether)}$ and 0.35S(4)$_{(thiolate)}$ + 0.65S(4)$_{(thioether)}$, respectively, were used in the refinement. Least-squares refinement of the positional and anisotropic thermal parameters of all of the non-hydrogen atoms and fixed-hydrogen atoms was based on F^2. A *SADABS* absorption correction was made.[17] The *SHELXTL* structure refinement program was employed.[18]

EPR Measurements. EPR measurements were performed at the X band using a Bruker EMX spectrometer equipped with a Bruker TE102 cavity. The microwave frequency was measured with a Hewlett-Packard 5246L electronic counter. The X-band EPR spectrum of **6** in THF was obtained with a microwave power of 19.922 mW (19.824 mW for **7**), a frequency of 9.602 GHz (9.604 GHz for **7**), and a modulation amplitude of 0.80 G at 100 kHz.

Acknowledgment. We gratefully acknowledge financial support from the National Science Council of Taiwan.

Supporting Information Available: X-ray crystallographic files in CIF format for the structure determinations of [PPN][Ni(SePh)(P(*o*-C_6H_3-3-$SiMe_3$-2-S)$_2$(*o*-C_6H_3−3-$SiMe_3$-2-SH))], [PPN][Ni(Cl)(P(*o*-C_6H_3-3-$SiMe_3$-2-S)$_2$(*o*-C_6H_3-3-$SiMe_3$-2-SH))], [Ni(P(*o*-C_6H_3-3-$SiMe_3$-2-S)$_2$(*o*-C_6H_3-3-$SiMe_3$-2-SH))]$_2$, [Ni(P(*o*-C_6H_3-3-$SiMe_3$-2-S)$_3$)]$_2$, [Na-18-crown-6-ether][Ni_2(P(*o*-C_6H_3-3-$SiMe_3$-2-S)$_3$)$_2$], [Ni_2(P(*o*-C_6H_3-3-$SiMe_3$-2-S)$_3$)(P(*o*-C_6H_3-3-$SiMe_3$-2-S)$_2$(*o*-C_6H_3-3-$SiMe_3$-2-SCH_3))], and [K-18-crown-6-ether]$_2$[Ni_2(P(*o*-C_6H_3-3-$SiMe_3$-2-S)$_3$)$_2$]. This material is available free of charge via the Internet at http://pubs.acs.org.

IC700719H

(17) Sheldrick, G. M. *SADABS, Siemens Area Detector Absorption Correaction Program*; University of Göttingen: Göttingen, Germany, 1996.

(18) Sheldrick, G. M. *SHELXTL, Program for Crystal Structure Determination*; Siemens Analytical X-ray Instruments Inc.: Madison, WI, 1994.